

Simple model for post seismic ionospheric disturbances above an earthquake epicentre and along connecting magnetic field lines

R. Marchand^{1,2} and J. J. Berthelier¹

¹CETP/IPSL, Saint-Maur-des-Fossés, France

²Department of Physics, University of Alberta, Canada

Received: 14 July 2008 – Revised: 8 October 2008 – Accepted: 8 October 2008 – Published: 8 December 2008

Abstract. The detection of ionospheric disturbances associated with seismic activity is one of the main objectives of the DEMETER micro-satellite. Its scientific payload provides a comprehensive set of electron and ion measurements. The present work describes a simple model of post-seismic disturbances in the ionosphere above the epicentre. Following a major seism, the neutral atmosphere is assumed to be subject to an acoustic pulse propagating upward, to high altitudes. By coupling this perturbation to the two-dimensional ionospheric model SAMI2 it is then possible to calculate the variations in a number of plasma parameters in the plume region and along connecting magnetic field lines, for an event of representative magnitude. The feasibility of identifying the signature of seismic events from satellite observations is then assessed in view of representative DEMETER measurements and of their natural variability.

1 Introduction

The human and economic impact of major earthquakes is such that considerable efforts are invested in understanding their causes, occurrence, and possible predictability. In addition to conventional ground based measurements, a number of interesting observations have been made in recent years, that correlate large seisms with perturbations in near Earth plasmas. Several statistical studies have presented cases for positive correlations between ionospheric disturbances taking place in conjunction with large earthquakes. While the question of earthquake predictability is still very much open for debate, the detection of ionospheric disturbances following large scale geophysical activity such as volcano eruptions

(Yong-Qiang et al., 2006), tsunamis (Gwal et al., 2006; Artru et al., 2005; Pavlov and Sukhorukov, 1987), seisms (Davies and Baker, 1965; Parrot et al., 1993; Calais and Minster, 1995; Gokov et al., 2002; Afraimovich et al., 2001; Gousheva et al., 2006), and high yield underground explosions (Kasymova and Zavoiskaya, 1989; Davies and Archambeau, 1998; Krasnov and Drobzheva, 2005), is now soundly established. Various types of disturbances have been observed following large earthquakes; including electromagnetic as well as plasma variations. The phenomena considered in this paper are the disturbances that affect the ionospheric plasma. One of our goals is to derive realistic amplitudes and timescales by considering model results and observations, and to assess the magnitude of the variations of the plasma parameters measured along the orbit of DEMETER (Parrot, 2002). In order to better concentrate on the basic phenomenology of the problem, we use a simplified model to describe the response of the neutral atmosphere to an earthquake. In this model, the vertical motion associated with a seism is assumed to lead to a plane acoustic pulse propagating vertically upward, up to the ionosphere. The neutral atmosphere is then coupled with the ionosphere using the two-dimensional SAMI2 ionospheric model. This model can be used to calculate the resulting plasma response directly above the epicentre, and along magnetic field lines connected to the plume region. The feasibility of recognising ionospheric seismic signatures is then assessed by comparing the calculated relative perturbations of several plasma parameters with their natural variability deduced from DEMETER observations.

The article is organised as follows. In Sect. 2 we present a simple gravity wave model used in the calculation. Section 3 briefly describes our ionospheric model and it presents results for plausible impulses in the neutral atmosphere resulting from large earthquakes. The natural variability in the measurements of ion temperatures and densities is considered in Sect. 4 in view of the feasibility of recognising



Correspondence to: R. Marchand
(richard.marchand@ualberta.ca)

specific seismic signatures of large earthquakes. Finally, the last section presents a general discussion of the results and some concluding remarks.

2 Model description

The propagation of acoustic gravity waves generated by earthquakes, up to ionospheric altitudes, has already been studied by a number of authors (e.g. Davies and Archambeau, 1998; Artru et al., 2004). In essence, the small amplitude (of order of a few mm) and long period (10–100 s) atmospheric oscillations generated at the ground level, propagate upward until they reach the ionosphere at altitudes 150–350 km, where coupling between the tenuous neutral atmosphere and the plasma leads to perturbations in the ionospheric profiles. A key element in this process is the exponential growth of the wave amplitude associated with the wave energy conservation, and the exponential decay in the background atmospheric neutral density. From energy balance considerations, it follows that the perturbed velocity associated with acoustic waves scales approximately as the reciprocal of the square root of the background density (Lognonné et al., 2006). This can be understood from the neutral continuity and momentum conservation equations

$$\frac{\partial}{\partial t}(\rho) + \frac{\partial}{\partial z}(\rho v) = 0, \quad (1)$$

and

$$\frac{\partial}{\partial t}(\rho v) + \frac{\partial}{\partial z}(\rho v v + \rho C_s^2) = -\rho g. \quad (2)$$

In writing Eq. (2), for simplicity, the atmosphere is assumed to be isothermal and the pressure is assumed to be related to the mass density through $p=C_s^2\rho$. Also, wave propagation is assumed to be purely vertical and the Coriolis force is neglected. It can be shown that these equations lead to

$$\frac{\partial}{\partial t}\left(\frac{\rho v^2}{2}\right) + \frac{\partial}{\partial z}\left(\frac{\rho v^2}{2}v\right) + v\left(C_s^2\frac{\partial\rho}{\partial z} + g\rho\right) = 0. \quad (3)$$

Making use of the fact that the last term in Eq. (3) vanishes at equilibrium, and assuming that, in the presence of an acoustic wave, relative perturbations in ρ are small, we see that Eq. (3) constitutes an approximate conservation equation for the wave kinetic energy. Thus, at altitudes of the order of 250 km, where the neutral density has decreased by a factor $\sim 10^{-10}$, the neutral velocity perturbation is amplified by $\sim 10^5$. For example, a large seism could give rise to a vertical displacement of ~ 1 cm with a period of ~ 10 – 100 s, corresponding to a vertical velocity $\sim 10^{-4}$ – 10^{-3} m/s at ground level. The corresponding perturbed velocity in the ionosphere, at ~ 250 km altitude, would therefore be of order 1–10 m/s, which corresponds to a vertical velocity perturbation of order 0.2–2% of the local sound speed. A detailed quantitative study of the effect of seismic activity on

the ionosphere at large distances from the epicentre would require coupling models for the propagation of surface waves on the solid Earth, with a gravity wave model of the neutral atmosphere, and with an ionospheric model. The first two steps of such a program have been reported by Lognonné et al. (1998). Also, in a recent paper and using a somewhat simplified model of the ionosphere, Shinagawa et al. (2007) applied a similar approach to the Sumatra earthquake of 26 December 2004. As a first step in understanding the physics involved in this problem, we postulate a plausible density impulse at ionospheric altitudes, and use the 2-D model of the ionosphere SAMI2 (Huba et al., 2000) to calculate the resulting perturbations in the surrounding plasma. To be specific, in the region where the tenuous neutral atmosphere and the ionosphere are effectively coupled, the impulse resulting from a seismic induced gravity wave is assumed to be described by a velocity perturbation

$$v_1 = \sqrt{2}V_0\frac{z-C_s t}{C_s\tau} \times \exp\left[\left(\frac{1}{2} + \frac{z-z_0}{2h}\right) - \frac{(z-z_0-C_s(t-t_0))^2}{C_s^2\tau^2}\right], \quad (4)$$

where V_0 is the maximum perturbed neutral atmosphere velocity at height h_0 , C_s is the local sound speed, h is the scale height of the neutral atmosphere, t_0 is the time at which the centre of the pulse reaches z_0 , and τ is the pulse duration. Considering that the main coupling between the neutral atmosphere and the ionospheric plasma takes places at altitudes ranging from 150 to 300 km, we use $h_0=250$ km in what follows and, for simplicity, we assume a constant sound speed of $C_s=600$ m/s. Referring to the MSIS model of the atmosphere (Schunk and Nagy, 2000), and considering the major species O only, we find that a representative value of h at that altitude is $h=41$ km. The corresponding perturbed density is estimated from the wave linearised continuity equation. Making use of the expression for v_1 given in Eq. (4), we find

$$\frac{\rho_1}{\rho_0} = \sqrt{2}\frac{V_0}{C_s}\left(\frac{z-C_s}{C_s\tau} + \frac{C_s\tau}{4h}\right) \times \exp\left[\left(\frac{1}{2} + \frac{z-z_0}{2h}\right) - \frac{(z-z_0-C_s(t-t_0))^2}{C_s^2\tau^2}\right] \quad (5)$$

The ionospheric model SAMI2 used in the simulations has been described in detail by Huba et al. (2000), and the interested reader is referred to this article for more details. In summary, the model solves the continuity and momentum equations for electrons and all ions species and the energy equations for electrons and the major ion species along the field lines in a given magnetic meridional plane. It accounts for photoionisation of the upper atmosphere by solar UV, and for several neutral and ion species (O, H and He being the most important). It also uses fits to the International Geomagnetic Reference Field (Maus et al., 2005) so that Earth

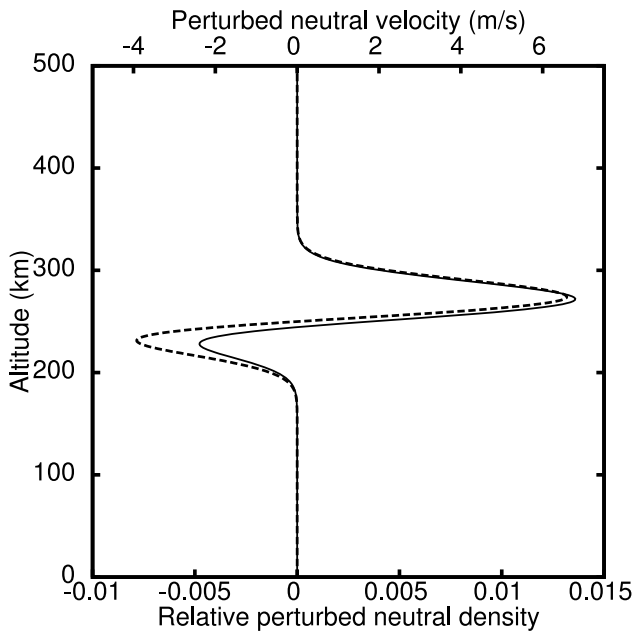


Fig. 1. Profile of the relative neutral density perturbation (solid – Eq. 5) and of the perturbed neutral atmosphere velocity (dotted – Eq. 4) associated with the imposed acoustic wave impulse.

magnetic field is not treated as a simple tilted excentric dipole field. SAMI2 also includes approximate empirical neutral wind and $E \times B$ drift models. These last two physical phenomena have been ignored in the calculations that follow, because their effects are not significant on the short time scales considered in this work.

3 2-D modelling of ionospheric perturbations

In this section the two-dimensional ionospheric model SAMI2 is used to assess the response of the ionosphere to a idealised acoustic wave impulse following an earthquake. Of the several parameters included in SAMI2, the electron density and temperature, and the ion velocity along field lines are those of main interest and will be shown here. The variations in these parameters are studied by comparing simulation results with and without the presence of the neutral acoustic pulse. Ionospheric plasma parameters are affected by the occurrence of a neutral acoustic wave in at least two ways. First, the local variation in density associated with the wave modifies the local ionisation production (collisional and, more importantly during the day, photoionisation). The second effect stems from the collisional drag of ions by neutral atoms and molecules that influences their motion parallel to the magnetic field. These two phenomena are, of course, indissociable in nature. Numerically, however, it is straightforward to include each effect separately in order to assess its relative importance. In this study, consistent with obser-

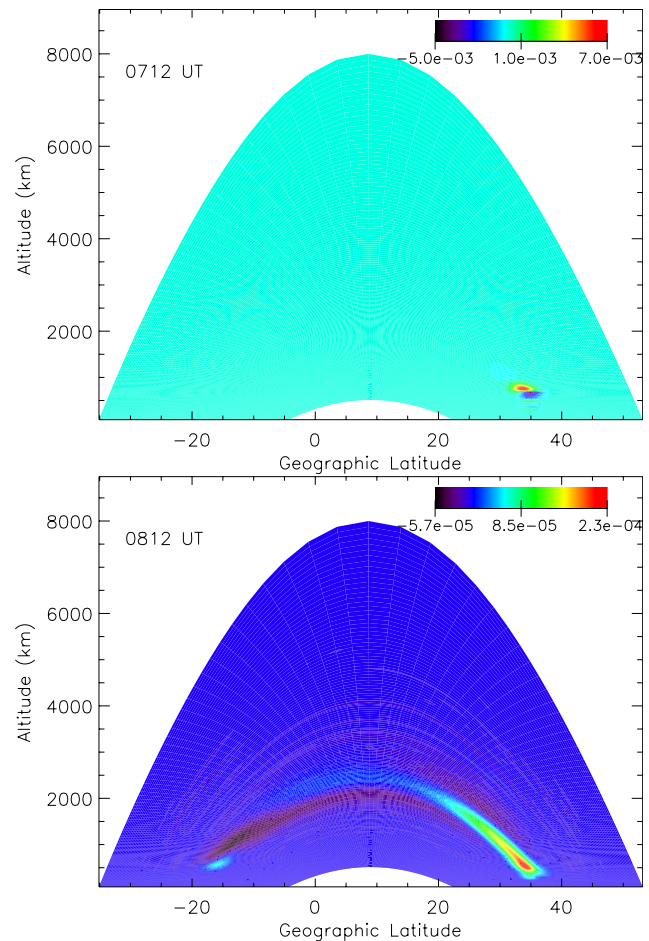


Fig. 2. Two-dimensional profiles of the relative density perturbation at 07:12 UT, shortly after the passage of the acoustic impulse, and at 08:12 UT. The relative density perturbation is the difference between the density calculated with and without the impulse, divided by the unperturbed density. The centre of the impulse reaches the altitude of 250 km at 07:00 UT.

vations (Artru et al., 2004), we assume an acoustic wave impulse that results in a maximum neutral velocity perturbation $V_0=5$ m/s at altitude $h_0=250$ km. From Eq. (5), this corresponds to a maximum relative density perturbation of 0.8% at h_0 . The impulse is triggered so that it reaches an altitude $h_0=250$ km at $t_0=13:00$ local time, near winter solstice, at latitude $\theta_0=35^\circ$ N, and longitude $\phi=90^\circ$. The impulse is assumed to be delimited in latitude by a Gaussian profile, with a half width $\Delta\theta=1.5^\circ$. For reference, the relative neutral density perturbation and velocity, at the time when the pulse reaches height h_0 , are shown in Fig. 1.

The effect of the acoustic impulse on the electron density is shown in Fig. 2, where the relative density perturbations are shown at two representative times following the acoustic pulse. The perturbation is strongest in the region where the variations in the neutral density and velocity associated with

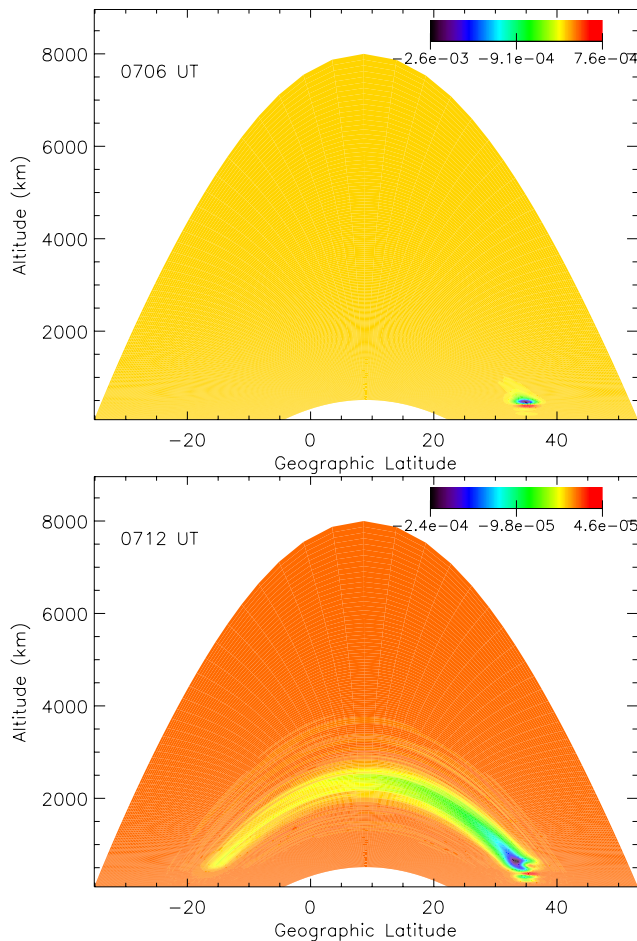


Fig. 3. Two-dimensional profiles of the relative temperature perturbation at 07:06, shortly after triggering the acoustic impulse, and at 07:12. The relative temperature perturbation is the difference between the temperature calculated with and without the impulse, divided by the unperturbed temperature.

the acoustic impulse, are largest. Numerically, the relative importance of the neutral density and velocity perturbations was assessed by artificially suppressing one contribution or the other. In our simulations, the response of the plasma parameters to the neutral density perturbation by itself is found to be smaller than that due to the velocity by a factor 5–10. All the results presented in the figures were obtained with both neutral density and velocity perturbations taken into account. It is nonetheless interesting to note that, for the conditions considered, the plasma perturbations are primarily determined by the atmospheric drag on the ions arising from the neutral velocity variations in the atmospheric wave pulse. Propagation of the plasma perturbation along the field line is associated, in part, with an ion acoustic wave driven by the passage of the acoustic wave impulse. It is also associated with the variation in electron temperature, which results from the acoustic wave, and the rapid electron thermal transport along field lines. As a consequence of this trans-

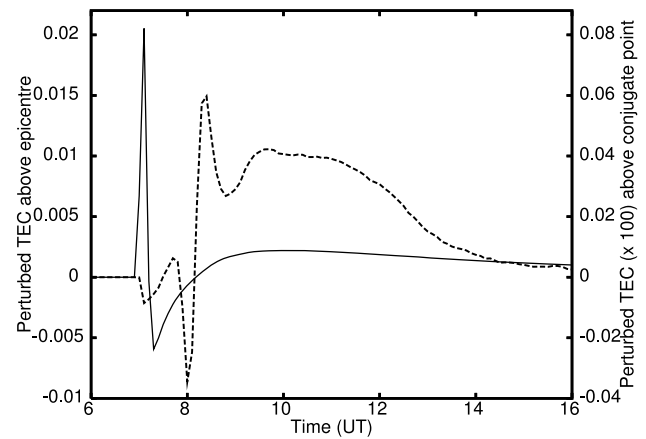


Fig. 4. Perturbed TEC in the plume region, at latitude $\theta=36^\circ$ N (solid), and close to the conjugate point (dashed), at $\theta\sim 16^\circ$ S. The perturbation is expressed in TEC units (10^{16} el/m $^{-2}$).

port, an appreciable perturbation appears to extend up to the conjugate point. The corresponding relative perturbation of the electron temperature is shown in Fig. 3. From the two solutions illustrated in these figures, it is clear that electron thermal diffusion along magnetic field lines is considerably faster than the propagation of the plasma density perturbation. Considering its propagation characteristics, the latter can likely be associated with the propagation of an ion acoustic wave along these lines. For reference, the ion acoustic velocity ranges from ~ 700 m/s at low altitudes ($h\sim 250$ km) to ~ 1500 km/s at higher altitudes (~ 2000 km). The corresponding variation in the TEC above the epicentre, and at its conjugate point ($\theta\sim 17^\circ$ S) is illustrated in Fig. 4. For the assumed amplitude of the acoustic impulse (~ 5 m/s at 250 km), the maximum TEC perturbation is approximately 0.02 TEC units (10^{16} m $^{-3}$) above the epicentre. A smaller (by a factor ~ 40) variation in TEC is also calculated at the conjugate point, with a delay of approximately 1 h. Above the epicentre, the TEC is seen to vary from a maximum, to a minimum value in approximately 30 min. At the conjugate point, TEC variations have more structure, and they evolve over a somewhat longer timescale. Another manifestation of these perturbations is seen in the variations of the plasma parallel velocity. To first approximation, the neutral atmosphere acoustic impulse only affects the magnetised ionospheric plasma in its dynamics along the magnetic field lines. The perturbation in the O $^+$ ion parallel velocity is shown in Fig. 5 at three times following the passage of the impulse. The field line selected joins the epicentre at latitude 35° N and its conjugate point at 17° S. The maximum perturbation calculated is of order 4 m/s at 07:00 UT; time at which the centre of the acoustic pulse reaches an altitude of 250 km. The perturbed velocity profiles plotted 12 and 18 min later show a combination of propagation, attenuation and dispersion along the field line.

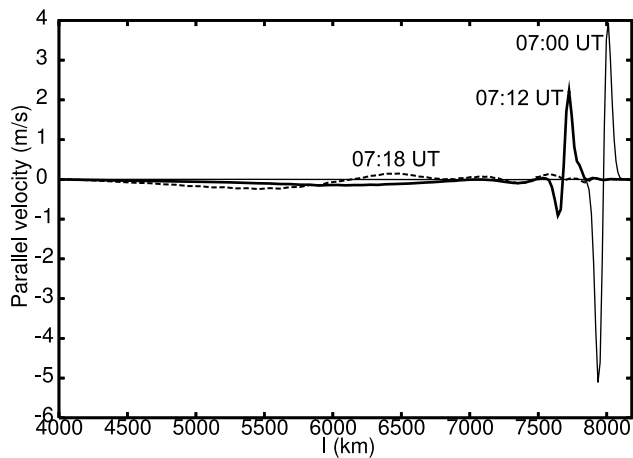


Fig. 5. Perturbed plasma parallel velocity calculated along a magnetic field line at different times after the passage of the acoustic impulse. The field line considered joins the epicentre at latitude 35° N to its conjugate point at 17° S. The distance l is measured along the field line, with $l=0$ being at the southern end.

4 Natural variability and measurability

At this point, it is appropriate to consider the feasibility of measuring the perturbations calculated with our model, and assess the feasibility of identifying them with seismic activity. As pointed out earlier, the analysis presented here is based on a number of simplifications, and the results are not intended to be comparable with detailed observations. The results should nonetheless be indicative of the type of perturbation that would result from a seismic induced acoustic wave, and the calculated amplitudes should provide an order of magnitude estimate of perturbation levels that would result from actual earthquakes. In order to be measurable, and be identified with a given seismic event, it is necessary for the plasma response to be of sufficient magnitude, so as to be clearly discriminated against otherwise natural ionospheric fluctuations and variations. The problem of identifying weak signals amongst a noisy or variable background is a difficult one, and it constitutes an area of active research in itself (Pilla et al., 2005). No attempt is made here to design measuring techniques or even to quantify the difficulty of making such measurements. It is nonetheless interesting to illustrate the difficulty involved by considering representative in situ measurements obtained with DEMETER. As an example of the variability of actual measurements, Fig. 6 shows five O^+ density traces measured along five consecutive day-side orbits near the winter 2006 solstice.

We note that DEMETER's quasi-heliosynchronous orbit passes at approximately 10:30 local time for day-side orbits. This is different from the local time of approximately 13:00 assumed in our calculations, but the corresponding difference in longitudes should have no significant effect on variability.

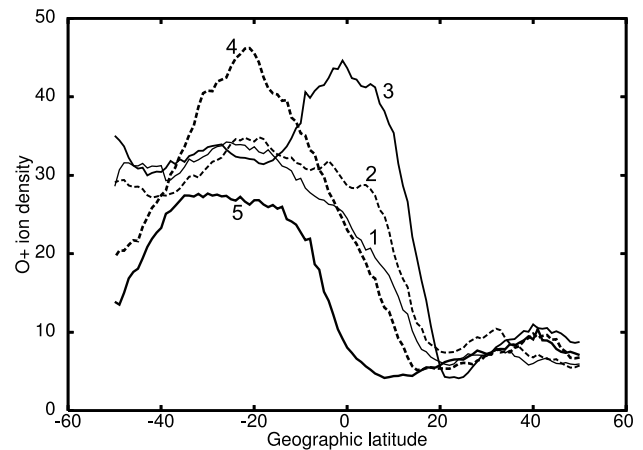


Fig. 6. Density of O^+ ions measured by DEMETER along five consecutive day orbits, near the winter solstice of 2007. Densities are in units of 10^9 m^{-3} , and numbers 1–5 indicate the chronological sequence of the orbits.

The figure illustrates the large variability in the O^+ density, which is representative of what would be found at other local times, and in other plasma parameters (in the electron and ion temperatures in particular). From that figure, it is clear that the calculated amplitudes of the perturbation resulting from an earthquake would be small compared with the natural variability of the plasma.

5 Conclusions

A model is presented to simulate the ionospheric effect of an upward propagating acoustic wave resulting from a large seismic event. Consistent with the near conservation of wave kinetic energy, the associated perturbed velocity is inversely proportional to the square root of the background atmospheric density. As a result, small ground displacements of the order of millimeters taking place over periods of tens of seconds, can lead to appreciable velocities of order of several meters per second, at altitudes where coupling between the neutral atmosphere and the ionosphere becomes important. The two-dimensional ionospheric model SAMI2 (Huba et al., 2000), is used to compute the response of the ionosphere to the assumed simplified acoustic impulse resulting from a large seism, and provide an order of magnitude estimate of the associated ionospheric density, temperature and velocity perturbations. For the amplitude of the acoustic wave assumed here, corresponding to a maximum perturbation in the neutral atmosphere velocity of 5 m/s at altitude 250 km, the perturbations in the ionosphere are most important above the epicentre, and they take place as the acoustic impulse reaches ionospheric altitudes (250–350 km). In the simulations, the maximum perturbation in the parallel velocity of O^+ ions is calculated to be of the order of 4 m/s. The

associated maximum relative perturbations in electron density and temperature are about 1% and 0.1%, respectively. A variation in the Total Electron Content (TEC) is also found to accompany these disturbances. With the acoustic impulse position and amplitude assumed in our model, the calculations yield a maximum TEC variation of approximately 0.02 TEC units (10^{16} m^{-3}) above the epicentre. Comparing with observed variations in the TEC following large earthquake (Afraimovich et al., 2005), we see that our predicted variations are smaller than observations by a factor ~ 5 –10. This quantitative difference is likely due to the amplitude of the acoustic pulse that we have considered and to the simplicity of our model; in particular, to the prescribed profile of the neutral atmosphere velocity and density perturbations. For the small amplitudes assumed here, the computed ionospheric response is approximately linear. A larger amplitude in the assumed acoustic perturbation would lead to a proportionally larger response in the ionospheric perturbation. Thus, by scaling the amplitude of our perturbation by a factor 5–10, we would obtain a perturbation in the TEC of approximately 0.1–0.2 TEC units, which would be in good agreement with observations. While oscillations in the TEC of order 0.1 have been observed, and correlated with seismic activity (Afraimovich et al., 2005), the scaled amplitudes of $3\text{--}6 \times 10^{-3}$ TEC units at the conjugate point, inferred from Fig. 4, would likely be too small to be measurable. A precise comparison with actual observations, in particular away from the epicentre region, would require coupling several models together, capable of simulating a variety of different phenomena. These would include a) the propagation of compressional and shear waves on Earth surface following a seismic activity, b) the coupling with (initially very low amplitude) low frequency acoustic wave in the neutral atmosphere, their propagation and amplification at high altitudes, and c) coupling with the ionosphere. Such a comprehensive study, addressed in part in earlier studies referred to in the introduction, is beyond the scope of the present analysis.

Acknowledgements. This work was supported in part, by CNES funding in the frame of the DEMETER project. One of us (RM) thanks the Natural Sciences and Engineering Research Council of Canada, the CNRS and the CETP for their financial support. This work uses the SAMI2 ionosphere model written and developed by the Naval Research Laboratory.

Edited by: P. F. Biagi

Reviewed by: E. L. Afraimovich and J.-M. Noel

References

- Afraimovich, E. L., Perevalova, N. P., Plotnikov, A. V., and Uralov, A. M.: The shock-acoustic waves generated by earthquakes, *Ann. Geophys.*, 19, 395–409, 2001, <http://www.ann-geophys.net/19/395/2001/>.
- Afraimovich, E. L., Astafieva, E. I., and Kiryushkin, V. V.: Ionospheric disturbance in the near-field area of the epicenter of the September 25, 2003 Hokkaido earthquake, *Radiophys. Quantum Electron.*, 48, 268–280, 2005.
- Artru, J., Farges, T., and Lognonné, P.: Acoustic waves generated from seismic surface waves: propagation properties determined from Doppler sounding observations and normal-mode modelling, *Geophys. J. Int.*, 158, 1067–1077, 2004.
- Artru, J., Ducic, V., Kanamori, H., Lognonné, P., and Murakami, M.: Ionospheric detection of gravity waves induced by tsunamis, *Geophys. J. Int.*, 160, 840–848, 2005.
- Calais, E. and Minster, J. B.: GPS detection of ionospheric perturbations following the January 1994, Northridge earthquake, *Geophys. Res. Lett.*, 22, 1045–1048, 1995.
- Davies, J. B. and Archambeau, C. B.: Modeling of atmospheric and ionospheric disturbances from shallow seismic sources, *Phys. Earth Planet. Inter.*, 105, 183–199, 1998.
- Davies, K. and Baker, D. M.: Ionospheric effects observed around the time of the Alaskan earthquake of March 28, 1964, *J. Geophys. Res.*, 70, 2251–2253, 1965.
- Gokov, A. M., Martynenko, S. I., Rozumenko, V. T., and Tyrnov, O. F.: Remote earthquake-induced large-scale ionospheric disturbances and strong mesospheric electric fields, *Telecommun. Radio Eng.*, 57, 136–140, 2002.
- Gousheva, M., Glavcheva, R., Danov, D., Angelov, P., Hristov, P., Kirov, B., and Georgieva, K.: Satellite monitoring of anomalous effects in the ionosphere probably related to strong earthquakes, *Adv. Space Res.*, 37, 660–665, 2006.
- Gwal, A. K., Shrivastava, A., and Malhotra, K.: Observation of seismogenic ultra low frequency electric field fluctuations detected as a burst in the ionosphere during tsunamis over the Andaman and Nicobar Islands, *Curr. Sci. (India)*, 91, 229–234, 2006.
- Huba, J. D., Joyce, G., and Fedder, J. A.: Sami2 is Another Model of the Ionosphere (SAMI2): A new low-latitude ionosphere model, *J. Geophys. Res.*, 105, 2335–2353, 2000.
- Kasymova, A. G. and Zavoiskaya, I. N.: Ionospheric effect of the Vrancea earthquake in Kiev, *Geofiz. Zh.*, 11, 76–80, 1989.
- Krasnov, V. M. and Drobzheva, Ya. V.: The acoustic field in the ionosphere caused by an underground nuclear explosion, *J. Atmos. Sol.-Terr. Phys.*, 67, 913–920, 2005.
- Lognonné, P., Clevede, E., and Kanamori, H.: Computation of seismograms and atmospheric oscillations by normal-mode summation for a spherical Earth model with realistic atmosphere, *Geophys. J. Int.*, 135, 388–406, 1998.
- Lognonné, P., Artru, J., Garcia, R., Crespon, F., Ducic, V., Jeansou, E., Occhipinti, G., Helbert, J., Moreaux, G., and Godet, P.-E.: Ground-based GPS imaging of ionospheric post-seismic signal, *Planet. Space Sci.*, 54, 528–540, 2006.
- Maus, S., Macmillan, S., Chernova, T., Choi, S., Dater, D., Golovkov, V., Lesur, V., Lowes, F., Luhr, H., Mai, W., McLean, S., Olsen, N., Rother, M., Sabaka, T., Thomson, A., and Zvereva, T.: The 10th generation International Geomagnetic Reference Field, *Phys. Earth Planet. Inter.*, 151, 320–322, 2005.
- Parrot, M.: The micro-satellite DEMETER, *J. Geodyn. (UK)*, 33, 535–541, 2002.
- Parrot, M., Achache, J., Berthelier, J. J., Blanc, E., Deschamps, A., Lefeuvre, F., Menvielle, M., Plantet, J. L., Tarits, P., and Villain, J. P.: High-frequency seismo-electromagnetic effects, *Phys. Earth Planet. Inter.*, 77, 65–83, 1993.
- Pavlov, V. I. and Sukhorukov, A. I.: Intermixing ionospheric disturbances caused by the propagation of tsunamis in the ocean, *Sov.*

- Tech. Phys. Lett., 13, 144–145, 1987.
- Pilla, R. S., Loader, C., and Taylor, C. C.: New technique for finding needles in haystacks: geometric approach to distinguishing between a new source and random fluctuations, *Phys. Rev. Lett.*, 95, 230 202–230 201, 2005.
- Schunk, R. and Nagy, A. F.: *Ionospheres Physics, Plasma Physics, and Chemistry*, Cambridge, 2000.
- Shinagawa, H., Iyemori, T., Saito, S., and Maruyama, T.: A numerical simulation of ionospheric and atmospheric variations associated with the Sumatra earthquake on 26 December 2004, *Earth Planets Space*, 59, 1015–1026, 2007.
- Yong-Qiang, H., Zuo, X., and Dong-He, Z.: Responses of the ionosphere to the Great Sumatra earthquake and volcanic eruption of Pinatubo, *Chin. Phys. Lett.*, 23, 1955–1957, 2006.